J Mater Sci (2006) 41:7838–7842
DOI 10.1007/s10853-006-0691-6

Spallation of single crystal nickel by void nucleation at shock induced grain junctions

S. G. Srinivasan · M. I. Baskes · G. J. Wagner

Received: 2 June 2006 / Accepted: 19 July 2006 / Published online: 24 October 2006

Abstract Molecular dynamics (MD) simulations of spallation in single crystal nickel were performed for a range of system sizes and impact velocities. The initial compressive wave leaves a rich microstructure in its wake. The subsequent tensile waves create multiple grains and grain junctions between regions of differing crystal orientation. These grain junctions serve as void nucleation sites when the reflected tensile waves interact, leading to ductile failure. In this way, the mechanism for failure in an initially single-crystalline sample is similar to that seen experimentally in high-purity, poly-crystalline metals, in which grain boundaries are sites for void nucleation.

Introduction

The phenomenon known as spallation can occur when a projectile hits a target at high velocity, causing compressive waves in both the target and the projectile. Upon reflection from free surfaces, these waves become tensile; the interaction of two reflected waves causes very high tensile stress resulting in material failure [1]. In metals, ductile spall failure typically initiates at nonmetallic inclusions, but Brandon et al. [2] found that in high purity copper the nucleation sites for failure are at the grain boundaries.

We are pleased to present results from our large-scale atomistic simulations of spallation in nickel for the Brandon Festschrift. Our simulations demonstrate a phenomenon, similar to what Brandon et al. discovered in polycrystalline copper [2], responsible for the spallation of single crystal nickel. Although there are initially no grain boundaries in our simulated material, we find that the passing of the first compressive shock wave through the material produces a rich microstructure, with regions of differing crystal structures and orientations. The grain boundaries between these regions become void nucleation sites when the reflected tensile waves interact, causing spall failure.

S. G. Srinivasan (✉) · M. I. Baskes
Materials Science & Technology, Los Alamos National Laboratory, MS: G755, MST-8 Group, Los Alamos, NM 87545, USA
e-mail: sgsrini@lanl.gov

G. J. Wagner
Sandia National Laboratories, Livermore, CA 94551, USA

Atomistic simulations and analyses

We performed a number of molecular dynamics (MD) simulations of spall in single crystal nickel. The geometry is shown schematically in Fig. 1. MD simulations involve numerical integration of Newton's equations of motion, over time, for an ensemble of interacting atoms. We used a time step size of 2 fs to evolve the system over time using the Nordseick numerical integration method [3].

Both the flyer plate and the target are blocks of Ni atoms, with the x-axis, which is the direction of impact, taken along the $<100>$-crystal direction. Periodic boundary conditions are imposed in the y and z directions, which correspond to $<110>$ directions in the crystal. The $\pm x$ surfaces are left free. The Ni atoms interact via an embedded atom method potential that has been fitted to the experimental

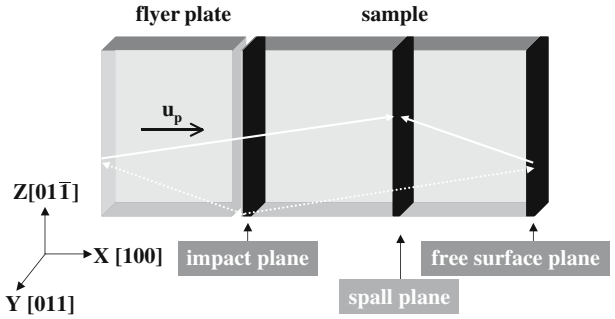

Fig. 1 A flyer plate with an initial velocity u_p slams into the sample. Impact creates compressive waves (shown by dotted white lines). Reflection of the compressive waves at the free surface yield tensile release waves (shown by continuous white lines). Release waves interact causing spall. We track stress, strain rate, and microstructure evolution near the impact, spall, and free surface planes

properties of nickel [3]. These properties are compared to experiments in Table 1.

The target and flyer are first thermalized at 300 K at a lattice constant appropriate to the system temperature. After equilibration, a relative velocity is assigned between the target and flyer along the *x* direction such that the center of mass velocity is zero, simulating high-velocity impact. Impact and subsequent time evolution were simulated without further temperature or pressure control at a constant energy.

The lengths of the systems we studied ranged from 3.2 nm to 3.52 μm, with cross-sectional areas between 2 and 125 nm^2. For all of our simulations, the length of the flyer plate was one-third that of the target, so that the resulting spall plane is midway between the impact plane and the free surface of the target. The smallest systems comprised a few hundred atoms, while the largest had 2.8 million atoms. Impact velocities ranged between 0.6 and 5.2 nm/ps.

Strain rates in experiments on spallation are typically estimated by measuring the free surface velocity as a function of time. In MD simulations, the strain rate ($\dot{\epsilon}$) can be either calculated from the free surface velocity, or evaluated directly from the bulk of the shocked specimen. We found that these two methods for computing the strain rate give different values for this quantity (S.G. Srinivasan et al., submitted); in order to draw comparisons with experiments we present values obtained using the surface velocity measurement. Surface velocity-measured strain rates in our simulations ranged from 10^8 to 10^{11} s^{-1}. Such strain rates can be attained experimentally using picosecond laser pulses [4], although experiments using explosively driven flyer plates are typically limited to strain rates $\leq 10^4$ s^{-1} [5, 6].

The local atomic structure in our sample was identified using the so-called Common Neighbor Analysis (CNA) algorithm [7]. We identified regions that clearly had FCC, BCC, and HCP structures; atoms in regions that did not fit these types were simply designated ''unknown''. Two adjacent layers of HCP atoms is the characteristic signature of an *intrinsic stacking fault*; one layer of HCP atoms separating FCC atom layers constitutes a *twin boundary*; and two HCP layers of atoms with one FCC layer in between indicate an *extrinsic stacking fault*.

Table 1 Comparison of material properties of nickel with those obtained using the embedded atom method (EAM) potential used in our simulations. EAM represents the properties of nickel very well

Properties	EAM	Experiment
Lattice constant (Å)	3.52	3.52
Cohesive energy (eV)	4.45	4.45
Vacancy formation energy (eV)	1.59	1.60
c_{11} (GPa)	246.4	246.5
c_{12} (GPa)	147.3	147.3
c_{44} (GPa)	124.8	124.7
Surface energy (J/m^2)	2.06	2.38
Stacking fault energy (mJ/m^2)	85	125

Results and discussion

The initial compressive impact wave produces a rich, complex, and dynamic microstructure in the simulated sample. Figure 2 shows the microstructural evolution in a single crystal Ni rod that eventually spalled. Samples with smaller in-plane dimensions show qualitatively similar microstructures upon shocking. Spallation occurred by nucleation and growth of voids in all the systems studied. In systems with small cross-sectional area, void nucleation and growth occurred rapidly within a fraction of a pico-second. On the other hand, we were able to follow void growth in larger systems over many tens of pico-seconds. In all samples, we were able to identify a threshold impact velocity or stress for spall. This limit is an upper limit of these quantities for void nucleation. We did not determine if void nucleation and collapse can occur below threshold, but it seems likely that it may.

We now examine the microstructural evolution near the impact plane. Initially, the compressive shock waves transform the FCC (green) structure to BCC (red) via a Bain transformation as shown in Fig. 2a. The shock fronts of the two compressive waves are clearly seen. The fraction of BCC atoms initially increases with time as shown in Fig. 2b. However, BCC

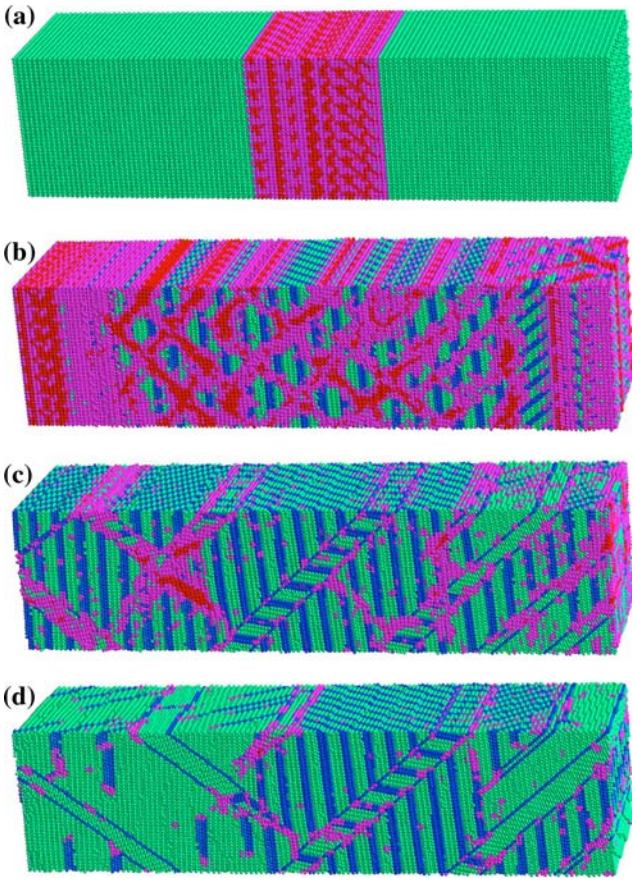

Fig. 2 Shock induced microstructural evolution in a single crystal Ni rod is shown over time. The rod's dimensions were $300 \times 11.4 \times 11.4$ nm^3 and initial particle velocity was 1.1 nm/ps. This view shows atoms within 20 nm on either side of the impact plane. Atoms are colored by their local crystallographic environment determined by CNA. Green, blue, red, and pink atoms are respectively FCC, HCP, BCC, and unknown atoms. (**a**)–(**d**) show atomic configurations at 0.5 ps, 2.5 ps, 7.5 ps, and 15 ps respectively

is unstable under the simulation conditions, and domains of BCC atoms revert to a defective FCC system with stacking faults (two layers of blue HCP atoms). At about 7.5 ps, as shown in Fig. 2c, we can see ordered domains with a rich and complex mosaic microstructure of FCC layers interwoven with stacking faults. Twin boundaries (identified by a single layer of HCP atoms) separate these domains. At 15 ps (Fig. 2d), the tensile release waves sweep through the volume. These waves destroy the rich microstructure created by the initial compressive waves. Now we are left with remnant point defects, isolated dislocation loops, and twin boundaries, as shown in the left half of Fig. 2d. Note that even though the very fine microstructure is removed by annihilation of dislocation dipoles, the remaining microstructure has a small characteristic size scale of ~ 1 nm. We are analyzing the effect of impact velocity on this length scale and it will be a topic for future work.

At the spall plane, the tensile waves transform the initially single-crystal structure to a rich polycrystalline microstructure as shown in Figure 3. A number of small grains are produced with their grain boundary normal generally parallel to the shock direction for the cases we analyzed. We do not know if this condition ensues for all cases. A number of cavities are nucleated at the newly formed grain boundaries and junctions when the peak tensile stress exceeds the spall strength. However, once a cavity starts to grow cavities in its neighborhood shrink and disappear. Figure 3 shows the nucleation of a cavity at a grain boundary junction. Nucleation and growth of the void is very rapid and occurs in <1 ps for all system sizes investigated. Some local amorphization of Ni in small regions is also visible; however, these regions rapidly crystallized during the spall process.

Figures 4 and 5 show the evolution of stress and temperature at the spall plane in the moments leading up to spallation failure in a $300 \times 1.4 \times 1.4$ nm^3 rod shocked by a flyer plate with particle velocities of 1.1 nm/ps. Figure 4a shows stress components and temperature near the spall plane at a simulation time of 55 ps. The hydrostatic stresses do not equal σ_{11} due

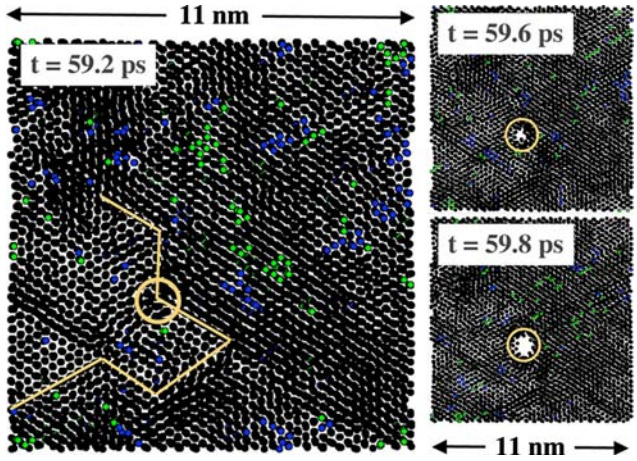

Fig. 3 Slices through the Ni rod at the spall plane. At 59.2 ps, we see a polycrystalline microstructure with grain boundaries marked by lines. The grain junction where a void will soon form is circled. At 59.6 ps, a void forms at the grain junction; it grows to ~ 1 nm at 59.8 ps. Void nucleation and growth occurs in <1 ps. At the spall plane, the interaction of the two tensile waves creates a rich microstructure and produces a very defective crystal. Thus, the CNA tags most of the atoms as unknown (colored black). We also see isolated clusters of FCC (green) and HCP (blue) atoms

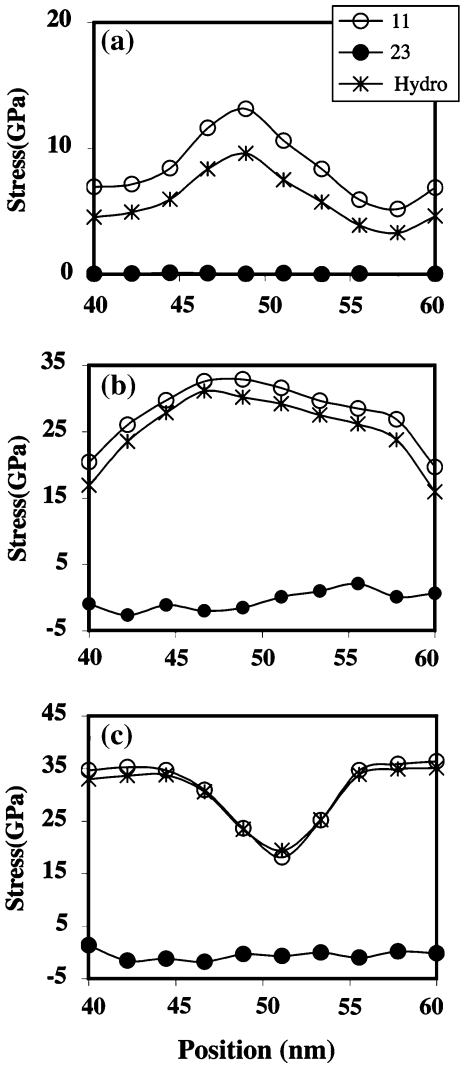

Fig. 4 Stresses as a function of x at the spall plane (x = ~ 50 nm). (**a**), (**b**), and (**c**) are plots at times 55 ps, 57 ps, and 59 ps respectively

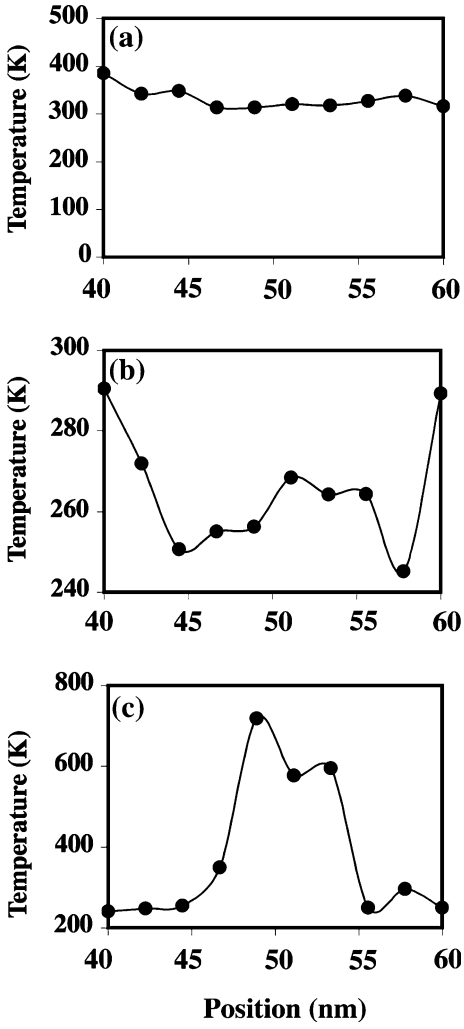

Fig. 5 Plot of temperature as a function of x at the spall plane (x = ~50 nm). (**a**), (**b**), and (**c**) are plots at times 55, 57, and 59 ps respectively

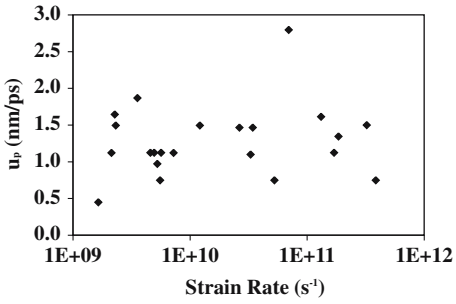

Fig. 6 Plot of shock velocity versus strain rate for spalled samples shows that the threshold velocity for spallation is independent of strain rate. The threshold velocity is between 0.5 and 2.0 nm/ps

to the presence of a persistent microstructure formed by the compressive shock waves. At t = 57 ps (Fig. b), the arrival of the tensile waves causes expansion of the system and a resultant cooling. Further, the interaction between these waves creates multiple grains and grain junctions between regions of differing crystal orientation. The material begins to fail by t = 57 ps (Figs. 4b, 5b), as voids are nucleated at grain boundaries and junctions; this cavitation causes heating and stress relief near the spall plane (Fig. 4c). In Fig. 4b, c, the shear stress σ_{23} is non-negligible, indicating the presence of a rich microstructure.

Figure 6 shows the shock velocity as a function of strain rates for the systems that spalled. It is clear that there exists a threshold velocity for void nucleation and growth. This threshold velocity appears to be independent of strain rate. The effects of strain rate on the threshold stress for spall will be presented elsewhere (S.G. Srinivasan et al., submitted).

Conclusions

We have studied spallation in single crystal nickel using large-scale MD simulations. These simulations have clarified the basic mechanism for spallation failure in a single crystal metal: the initial compressive shock wave imparts a rich microstructure; tensile waves from the free-surfaces remove most of the initial microstructure; interaction of tensile waves at the spall plane create crystals with different orientation and their boundaries become nucleation sites for voids. Subsequent void growth and coalescence leads to ductile failure. The junctions in the newly formed microstructure play the same role as the grain boundaries in high-purity, polycrystalline copper studied by Brandon et al. [2].

Acknowledgements This work was funded by the ASC program at the Los Alamos National Laboratory. Sandia is a multi program laboratory operated by Sandia Corporation, a Lockheed Martin Company, for the United States Department of Energy's National Nuclear Security Administration under contract DEAC04-94AL85000. Many of the calculations were performed on the LANL QSC parallel computer using a modified version of Warp, a molecular dynamics code originally developed by Steve Plimpton at Sandia.

References

1. Gray GT III (2000) ASM Handbook 8:530
2. Brandon DG, Boas M, Rosenberg Z (1984) Proc. of the 3rd Conf. on the Mech. Prop. of Mater. at High Rates of Strain, 9–12 April 1984, Oxford, UK; p 261
3. Angelo JE, Moody NR, Baskes MI (1995) Model Simul Mater Sci Engg 3:289; Baskes MI, Sha XW, Angelo JE, Moody NR (1997) ibid 5:651
4. Dekel E, Eliezer S, Henis Z, Moshe E, Ludmirsky A, Goldberg IB (1998) J Appl Phys 84:4851
5. Follansbee PS, Gray GT III (1991) Inter J Plast 7:651
6. Baumung K, Bluhm H, Kanel GI, Müller G, Razorenov SV, Singer J, Utkin AV (2001) Inter J Impact Engg 24:631
7. Jónsson H, Andersen HC (1988) Phys Rev Lett 60:2295